Impact ionization coefficients of 4H silicon carbide

T. Hatakeyama,[a] T. Watanabe, and T. Shinohe
Corporate R&D Center, Toshiba Corporation, 1, Komukai Toshiba-cho, Saiwai-ku, Kawasaki 212-8582, Japan

K. Kojima and K. Arai
National Institute of Advanced Industrial Science and Technology, Tsukuba Center 2, 1-1-1 Umezono, Tsukuba, Ibaraki 305-8568, Japan

N. Sano
Institute of Applied Physics, University of Tsukuba, 1-1-1 Tennodai, Tsukuba, Ibaraki 305-8577, Japan

(Received 2 March 2004; accepted 21 June 2004)

Anisotropy of the impact ionization coefficients of 4H silicon carbide is investigated by means of the avalanche breakdown behavior of p^+n diodes on (0001) and $(11\bar{2}0)$ 4H silicon carbide epitaxial wafers. The impact ionization coefficients are extracted from the avalanche breakdown voltages and the multiplication of a reverse leakage current, due to impact ionization of these p^+n diodes. The breakdown voltage of a p^+n diode on a $(11\bar{2}0)$ wafer is 60% of that on a (0001) wafer, and the extracted impact ionization coefficients of 4H silicon carbide show large anisotropy. We have shown that the anisotropy of the impact ionization coefficients is related to the anisotropy of carrier heating and drift velocity, which are due to the highly anisotropic electronic structure of 4H silicon carbide. © *2004 American Institute of Physics*. [DOI: 10.1063/1.1784520]

Among many wide band-gap semiconductor materials, 4H silicon carbide (4H-SiC) has great potential for use as the material for power devices, owing to its crystal maturity and superior electrical properties, such as nearly isotropic mobility and high breakdown electric field. Impact ionization coefficients are important material properties for power devices, because the avalanche breakdown of a power device is caused by the impact ionization phenomena, and the physical model of an impact ionization coefficient is indispensable for the device simulation of power devices. However, the reports of measurements of the impact ionization coefficient of 4H-SiC are few, and they are not in agreement with one another.[1,2] Recently, it was shown that a significant reduction of the breakdown field in 4H-SiC occurs when the electric field is applied perpendicular to the *c*- axis, but the impact ionization coefficients were not reported.[3] In order to predict the breakdown voltage of a real power device precisely, we have to consider the anisotropy of impact ionization coefficients, because the direction of the electric field at the field crowding part is not necessarily parallel to the *c* axis when the reverse bias is applied, even if the device is fabricated on a (0001) 4H-SiC wafer.

In this letter, we present the impact ionization coefficients of 4H-SiC for $\langle 0001 \rangle$ and $\langle 11\bar{2}0 \rangle$ directions that reproduce avalanche breakdown behavior of p^+n diodes on (0001) and $(11\bar{2}0)$ epitaxial 4H-SiC wafers. We also discuss the origin of anisotropy of the impact ionization coefficient of 4H-SiC, based on the microscopic description of the impact ionization and the transport physics under high electric field.

The breakdown voltages as a function of doping density and the multiplication factors of a leakage current were obtained using p^+n diode fabricated on (0001) and $(11\bar{2}0)$ epitaxial 4H-SiC wafers. The substrates used in this work were heavily doped *p*-type (0001) and $(11\bar{2}0)$ 4H-SiC wafers purchased from Cree Research, Inc. The epitaxial layers on a (0001) wafer were grown by Cree Research, Inc., and those on a $(11\bar{2}0)$ wafer were grown in a horizontal hot-wall chemical-vapor deposition reactor using SiH_4 and C_3H_8 as source gases and H_2 as a carrier gas.[4] The inset of Fig. 1 shows a cross section of the p^+n diode and the measuring system for multiplication factors. The p^+n junction of a diode is located between a p^+-type epitaxial layer, on a p^+-type substrate and an *n*-type epitaxial layer in order to exclude the effect of defects in the substrate. The doping concentration of the *n*-type epitaxial layer, was between 3×10^{16} and 2×10^{17} cm^{-3}. Deep mesa for the isolation and termination of p^+n diodes was formed using inductively coupled plasma reactive ion etching in SF_6 chemistries. Nickel was deposited for the contact area after the contact implantation and

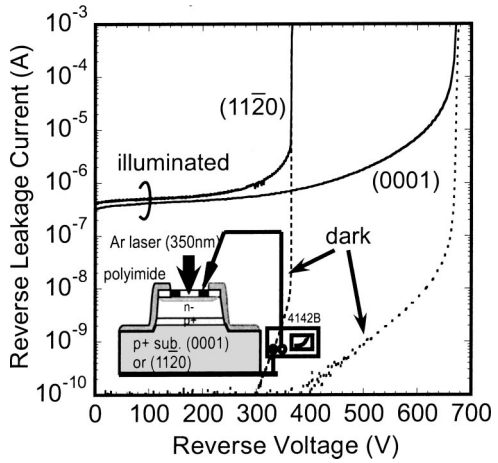

FIG. 1. Reverse leakage current of p^+n diodes on (0001) and $(11\bar{2}0)$ wafers in the dark and in UV light. The inset shows a cross section of the p^+n diode and the measuring system for multiplication factors.

[a]Electronic mail: tetsuo2.hatakeyama@toshiba.co.jp

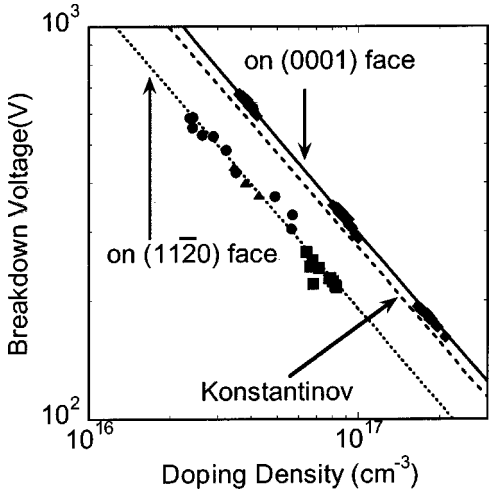

FIG. 2. Measured results of the avalanche breakdown voltages for p^+n diodes on (0001) and (11$\bar{2}$0) wafers as a function of doping density of the n-type epitaxial layer.

1600 °C activation annealing, and sintered before the metalization. Last, photosensitive polyimide was coated and patterned as a passivation layer. This passivation layer is effective for avoiding air spark formation. The active area of a diode is circular, in order to prevent field crowding at the corner. The diameter of a mesa diode is 500 μm. The thickness of the n-type epitaxial layer is 10 μm, which is thick enough to prevent the depleting region from reaching the substrate when the reverse bias is applied. Reverse current-voltage characteristics of p^+n diodes were measured using agilent 4142B. Photomultiplication factors were calculated from the reverse leakage current versus voltage characteristics under the illumination of UV light using an Ar laser ($\lambda = 350$ nm). Figure 1 shows a the reverse leakage current of p^+n diodes on (0001) and (11$\bar{2}$0) wafers in the dark and in the UV light. The doping density of the n^- epitaxial layer for both samples is approximately 4×10^{16} cm^{-3} The breakdown voltage of a p^+n diode on a (11$\bar{2}$0) wafer is 50%–60% of that on a (0001) wafer. It should be noted that a p^+n diode on (11$\bar{2}$0) shows very small leakage current to the avalanche breakdown voltage. Most p^+n diodes on (11$\bar{2}$0) wafers did not show a small leakage current, as indicated in Fig. 1.

From Fig. 1, we can also see that the multiplication factor of a p^+n diode on (11$\bar{2}$0) is smaller than that of a p^+n diode on (0001). This means that the imbalance between the hole-impact ionization coefficient (β) and the electron-impact ionization coefficient (α) is small compared with the case of (0001) face, as shown later.

Figure 2 shows the measured results of the avalanche breakdown voltages for p^+n diodes on (0001) and (11$\bar{2}$0) 4H-SiC wafers as a function of doping density of the n-type epitaxial layer. In Fig. 2, the result for Ref. 1 is shown for the purpose of comparison. The doping-dependent breakdown voltage of p^+n diodes on the (0001) wafer is 10% larger than that in Ref. 1. The breakdown voltage of the p^+n diodes is expressed by the following formula: $V_{BD}=1940\times(10^{16}/N_D)^{0.8}$ for a (0001) face and $V_{BD}=1200\times(10^{16}/N_D)^{0.8}$ for a (11$\bar{2}$0) face. The breakdown voltage of a p^+n diode on a (11$\bar{2}$0) wafer is 60% of that on a (0001) wafer in the case that the doping density of the epitaxial layer is the same. Thus, in designing the structure of power devices made of 4H-SiC, it is necessary to pay attention to the direction of the high electric field when the reverse voltage is applied.

TABLE I. Parameters of the electron- and hole-impact ionization coefficients of 4H-SiC.

Parameter	⟨0001⟩	⟨11$\bar{2}$0⟩
a_e(cm^{-1})	1.76×10^8	2.10×10^7
b_e(V/cm)	3.30×10^7	1.70×10^7
a_h(cm^{-1})	3.41×10^8	2.96×10^7
b_h(V/cm)	2.50×10^7	1.60×10^7

The impact ionization coefficients are obtained by the combined fitting procedure of the multiplication versus voltage characteristics and breakdown voltage-doping density curve, as mentioned above. The impact ionization coefficient model commonly used in the device simulator is based on the model suggested by Chynoweth:[5] $\alpha=a_e\exp(-b_e/F)$, $\beta=a_h\exp(-b_h/F)$, where F represents the magnitude of the electric field. Other parameters are fitting parameters. The calibrated parameters of the electron- and hole-impact ionization coefficients model are summarized in Table I. Figure 3 shows the obtained impact ionization coefficients in ⟨0001⟩ direction and those in ⟨11$\bar{2}$0⟩ direction. It can be seen that the ionization coefficients in ⟨11$\bar{2}$0⟩ direction are larger than those in ⟨0001⟩ direction. Further, the asymmetry of the electron and hole-ionization coefficients in ⟨11$\bar{2}$0⟩ direction is smaller than that in ⟨0001⟩ direction.

Now we discuss the origin of the anisotropy of the impact ionization coefficients of 4H-SiC from the physical and theoretical points of view. The impact ionization coefficient for electrons is expressed by the integral of the product of the impact ionization rate and distribution function,

$$\alpha=\frac{1}{nv_d}\int_0^\infty dE w_{ii}(E)f(E)\rho(E), \tag{1}$$

where n, v_d, $f(E)$, $w_{ii}(E)$, and $\rho(E)$ denote electron density, drift velocity, distribution function, impact ionization rate, and density of states, respectively.[6] Impact ionization for holes can be viewed as a mirror image of the impact ioniza-

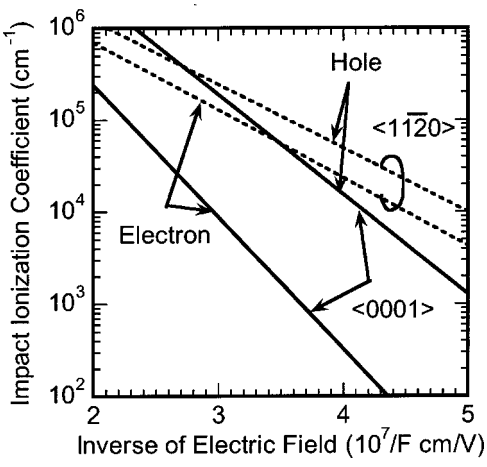

FIG. 3. Measured impact ionization coefficients in the ⟨0001⟩ direction and those in the ⟨11$\bar{2}$0⟩ direction.

tion for electrons, and so we treat only the electron impact ionization. The Keldysh formula is assumed for the impact ionization rate

$$w_{ii}(E) = C_{ii}(E - E_{\mathrm{th}})^{\alpha}, \tag{2}$$

where E_{th} is a threshold energy and C_{ii} is a fitting parameter.[7,8] The distribution function $f(E)$ is a solution of the Boltzmann transport equation (BTE), which includes microscopic physical properties, such as the band-structure and carrier scattering mechanisms. For easier comprehension, we first adopt the "hydrodynamic" model to introduce the mean quantities, such as carrier temperature and drift velocity, and their relation with impact ionization coefficients.[9] The BTE is treated as a set of the kinetic equations for mean quantities in the hydrodynamic model. After we can figure out the relation between the mean quantities and impact ionization coefficients, we return to the discussion of the effect of microscopic physical properties on high-field transport. In the hydrodynamic model, the distribution function is assumed to be nearly Maxwellian:

$$f(E) = \exp(-E/k_B T_e), \tag{3}$$

where T_e is an electron temperature, or electron mean energy. The relation between the electron temperature and the drift velocity is derived from the energy balance equation, which is one of the kinetic equations in the hydrodynamic model:

$$k_B T_e = k_B T_L + \tfrac{2}{3} e(v_d \tau_w) F \approx \tfrac{2}{3} e(v_d \tau_w) F \quad \text{for} \quad F \gg 1, \tag{4}$$

where T_L and τ_w denote lattice temperature and energy relaxation time. Equations (1)–(3) indicate that the impact ionization coefficient depends exponentially on the carrier temperature, because hot carriers that have a larger energy than E_{th} contribute to the impact ionization coefficient. If the carrier temperature varies according to the direction of the electric field, the impact ionization coefficient should be anisotropic. Further, from Eq. (4), if the drift velocity under high electric field is anisotropic, the impact ionization coefficient should be anisotropic. The anisotropies of these quantities are related to each other. However, we have to emphasize that the anisotropy of mean quantity itself cannot be derived in the framework of the hydrodynamic model. In order to identify the origin of the anisotropy of the mean quantities, we have to evaluate the effect of microscopic physical properties on high-field transport using the BTE, which is directly solved by the Monte Carlo technique, considering the band-structure and carrier scattering mechanisms. Monte Carlo studies of high-field transport in 4H-SiC have shown anisotropy of the carrier velocity, the carrier temperature and the impact ionization coefficients; the carrier velocity, the carrier temperature, and the impact ionization coefficients under the electric field parallel to the *c* axis are much smaller than those under the electric field perpendicular to the *c* axis.[10–12] This is due to the highly anisotropic band structure of 4H-SiC, which is derived from a long period along the *c* axis of the crystal structure of 4H-SiC.

The anisotropy of the saturation velocity can be estimated from anisotropy of the impact ionization coefficients based on Eq. (4), if we assume that the drift velocity shows saturation characteristics as for the electric field. The electron saturation velocity parallel to the *c* axis is about 60% of that perpendicular to the *c* axis. The hole saturation velocity parallel to the *c* axis is about 80% of that perpendicular to the *c* axis.

In conclusion, the electric-field dependence and anisotropy of the impact ionization coefficients of 4H-SiC are obtained. The obtained impact ionization coefficients show large anisotropy; the ionization coefficients in $\langle 11\bar{2}0 \rangle$ direction are larger than those in the $\langle 0001 \rangle$ direction and the asymmetry of the electron and hole-ionization coefficients in the $\langle 0001 \rangle$ direction is smaller than that in the $\langle 11\bar{2}0 \rangle$ direction. The anisotropy of the impact ionization coefficients is originated from the anisotropic electronic structure or crystal structure of 4H-SiC.

This work was performed under the management of FED as part of a Ministry of Economy, Trade and Industry (METI) Project (R&D Research and Development of Ultra-Low-Loss Power Device Technologies) supported by the New Energy and Industrial Technology Development Organization (NEDO).

[1] A. O. Konstantinov, Q. Wahab, N. Nordell, and U. Lindefelt, Appl. Phys. Lett. **71**, 90 (1997).
[2] R. Raghunathan and B. J. Baliga, Solid-State Electron. **43**, 199 (1999).
[3] S. Nakamura, H. Kumagai, T. Kimoto, and H. Matsunami, Appl. Phys. Lett. **80**, 3355 (2002).
[4] K. Kojima, T. Ohno, T. Fujimoto, M. Katsuno, N. Ohtani, J. Nishio, Y. Ishida, T. Takahashi, T. Suzuki, T. Tanaka, and K. Arai, Appl. Phys. Lett. **81**, 2974 (2002).
[5] A. G. Chynoweth, Phys. Rev. **109**, 1537 (1958).
[6] A. Schenk, *Advanced Physical Models for Silicon Device Simulation* (Springer, Wien, 1998), p. 90.
[7] L. V. Keldysh, Zh. Eksp. Teor. Fiz. **48**, 1962 (1965) [Sov. Phys. JETP **21**, 1135 (1965)].
[8] K. Hess, *Monte Carlo Device Simulation: Full Band and Beyond* (Klumer, Boston, 1991), Chap. 2.
[9] K. Bløtekjaer, IEEE Trans. Electron Devices **17**, 38 (1970).
[10] H.-E. Nilsson and M. Hjelm, J. Appl. Phys. **86**, 6230 (1999).
[11] E. Bellotti, H.-E. Nilsson, K. F. Brennan, P. P. Ruden, and R. Trew, J. Appl. Phys. **87**, 3864 (2000).
[12] M. Hjelm, H.-E. Nilsson, A. Martinez, K. F. Breman, and E. Bellotti, J. Appl. Phys. **93**, 1099 (2003).